Supporting Information for "Dilution of boundary layer cloud condensation nucleus concentrations by free tropospheric entrainment during marine cold air outbreaks"

F. Tornow[1,2], A. S. Ackerman[2], A. M. Fridlind[2], B. Cairns[2], E. C. Crosbie[3,4],

S. Kirschler[5,6], R. H. Moore[3], C. E. Robinson[3,4], C. Seethala[7], M. A. Shook[3],

C. Voigt[5,6], E. L. Winstead[3,4], L. D. Ziemba[3], P. Zuidema[7], A. Sorooshian[8,9]

[1]Earth Institute, Columbia University, NY, 10025, NY

[2]NASA Goddard Institute for Space Studies, NY, 10025, NY

[3]NASA Langley Research Center, Hampton, VA 23681, USA

[4]Science, Systems, and Applications, Inc., Hampton, VA 23681, USA

[5]Deutsches Zentrum für Luft- und Raumfahrt (DLR), Oberpfaffenhofen, Germany

[6]Johannes Gutenberg-Universität, Mainz, Germany

[7]Rosenstiel School of Marine and Atmosphere Science, University of Miami, FL, 33149, USA

[8]Department of Chemical and Environmental Engineering, University of Arizona, Tucson, Arizona, 85721, USA

[9]Department of Hydrology and Atmospheric Sciences, University of Arizona, Tucson, Arizona, 85721, USA

Contents of this file

2. Tables S1 to S2

References

Burton, S. P., Hostetler, C. A., Cook, A. L., Hair, J. W., Seaman, S. T., Scola, S., ... Müller, D. (2018, Jul). Calibration of a high spectral resolution lidar using a michelson interferometer, with data examples from oracles. *Appl. Opt.*, *57*(21), 6061–6075. Retrieved from http://www.osapublishing.org/ao/abstract.cfm?URI=ao-57-21-6061 doi: 10.1364/AO.57.006061

Cairns, B., Russell, E. E., & Travis, L. D. (1999). Research Scanning Polarimeter: calibration and ground-based measurements. In D. H. Goldstein & D. B. Chenault (Eds.), *Polarization: Measurement, analysis, and remote sensing ii* (Vol. 3754, pp. 186 – 196). SPIE. Retrieved from https://doi.org/10.1117/12.366329 doi: 10.1117/12.366329

DeCarlo, P. F., Dunlea, E. J., Kimmel, J. R., Aiken, A. C., Sueper, D., Crounse, J., ... Jimenez, J. L. (2008). Fast airborne aerosol size and chemistry measurements above mexico city and central mexico during the milagro campaign. *Atmospheric Chemistry and Physics*, *8*(14), 4027–4048. Retrieved from https://acp.copernicus.org/articles/8/4027/2008/ doi: 10.5194/acp-8-4027-2008

Froyd, K. D., Murphy, D. M., Brock, C. A., Campuzano-Jost, P., Dibb, J. E., Jimenez, J.-L., ... Ziemba, L. D. (2019). A new method to quantify mineral dust and other aerosol species from aircraft platforms using single-particle mass spectrometry. *Atmospheric Measurement Techniques*, *12*(11), 6209–6239. Retrieved from https://amt.copernicus.org/articles/12/6209/2019/ doi: 10.5194/amt-12-6209-2019

Hock, T. F., & Franklin, J. L. (1999). The ncar gps dropwindsonde. *Bulletin of the American Meteorological Society*, *80*(3), 407 - 420. Retrieved from https://journals.ametsoc.org/view/journals/bams/80/3/1520-0477_1999_080_0407_tngd_2_0_co_2.xml doi: 10.1175/1520-0477(1999)080⟨0407:TNGD⟩2.0.CO;2

Kleine, J., Voigt, C., Sauer, D., Schlager, H., Scheibe, M., Jurkat-Witschas, T., ... Anderson, B. E. (2018). In situ observations of ice particle losses in a young persistent contrail. *Geophysical Research Letters*, *45*(24), 13,553-13,561. Retrieved from https://agupubs.onlinelibrary.wiley.com/doi/abs/10.1029/2018GL079390 doi: https://doi.org/10.1029/2018GL079390

Knop, I., Bansmer, S. E., Hahn, V., & Voigt, C. (2021). Comparison of different droplet measurement techniques in the braunschweig icing wind tunnel. *Atmospheric Measurement Techniques*, *14*(2), 1761–1781. Retrieved from https://amt.copernicus.org/articles/14/1761/2021/ doi: 10.5194/amt-14-1761-2021

Lance, S., Nenes, A., Medina, J., & Smith, J. N. (2006). Mapping the operation of the dmt continuous flow ccn counter. *Aerosol Science and Technology*, *40*(4), 242-254. Retrieved from https://doi.org/10.1080/02786820500543290 doi: 10.1080/02786820500543290

Lawson, R. P., O'Connor, D., Zmarzly, P., Weaver, K., Baker, B., Mo, Q., & Jonsson, H. (2006). The 2d-s (stereo) probe: Design and preliminary tests of a new airborne, high-speed, high-resolution particle imaging probe. *Journal of Atmospheric and Oceanic Technology*, *23*(11), 1462 - 1477. Retrieved from https://journals.ametsoc.org/

view/journals/atot/23/11/jtech1927_1.xml doi: 10.1175/JTECH1927.1

Moore, R. H., Thornhill, K. L., Weinzierl, B., Sauer, D., D'Ascoli, E., Kim, J., ... Anderson, B. E. (2017). Biofuel blending reduces particle emissions from aircraft engines at cruise conditions. *Nature*, *543*, 411-415. Retrieved from https://www.nature.com/articles/nature21420 doi: 10.1038/nature21420

Rolph, G., Stein, A., & Stunder, B. (2017). Real-time environmental applications and display system: Ready. *Environmental Modelling & Software*, *95*, 210-228. Retrieved from https://www.sciencedirect.com/science/article/pii/S1364815217302360 doi: https://doi.org/10.1016/j.envsoft.2017.06.025

Sorooshian, A., Brechtel, F. J., Ma, Y., Weber, R. J., Corless, A., Flagan, R. C., & Seinfeld, J. H. (2006). Modeling and characterization of a particle-into-liquid sampler (pils). *Aerosol Science and Technology*, *40*(6), 396-409. Retrieved from https://doi.org/10.1080/02786820600632282 doi: 10.1080/02786820600632282

Stein, A. F., Draxler, R. R., Rolph, G. D., Stunder, B. J. B., Cohen, M. D., & Ngan, F. (2015). Noaa's hysplit atmospheric transport and dispersion modeling system. *Bulletin of the American Meteorological Society*, *96*(12), 2059 - 2077. Retrieved from https://journals.ametsoc.org/view/journals/bams/96/12/bams-d-14-00110.1.xml doi: 10.1175/BAMS-D-14-00110.1

Taylor, J. W., Haslett, S. L., Bower, K., Flynn, M., Crawford, I., Dorsey, J., ... Coe, H. (2019). Aerosol influences on low-level clouds in the west african monsoon. *Atmospheric Chemistry and Physics*, *19*(13), 8503–8522. Retrieved from https://acp.copernicus.org/articles/19/8503/2019/ doi: 10.5194/acp-19-8503-2019

Tornow, F., Ackerman, A. S., & Fridlind, A. M. (2021). Preconditioning of overcast-to-broken cloud transitions by riming in marine cold air outbreaks. *Atmospheric Chemistry and Physics*, *21*(15), 12049–12067. Retrieved from https://acp.copernicus.org/articles/21/12049/2021/ doi: 10.5194/acp-21-12049-2021

Table S1. 2020 ACTIVATE CAO research flights, the prevalent MBL wind direction, coordinates defining the initial cloud edge, and instrument limitations relevant to this study (see text).

Date / Leg	#	Wind Dir.	Cloud edge coordinates	Instrument Limitations
2020-02-21 / 1	RF04	20°	38.0°N 76.4°W – 39.5°N 72.0°W	Falcon only
2020-02-22 / 1	RF05	25°	34.0°N 77.4°W – 38.0°N 71.5°W	Falcon only
2020-02-22 / 2	RF06	25°	34.0°N 77.4°W – 38.0°N 71.5°W	Falcon only
2020-02-27 / 1	RF09	300°	34.0°N 76.0°W – 38.0°N 73.0°W	/
2020-03-01 / 1	RF13	315°	35.0°N 75.0°W – 40.0°N 72.0°W	/
2020-03-01 / 2	RF14	315°	35.0°N 74.0°W – 40.0°N 72.0°W	/
2020-03-08 / 1	RF17	10°	33.0°N 77.0°W – 36.5°N 72.0°W	No RSP
2020-03-08 / 2	RF18	20°	34.5°N 78.0°W – 34.5°N 70.0°W	No RSP

Table S2. Instruments, products, and estimated uncertainty used.

Instrument (in-situ)	**Used Products**	**Uncertainty**	**Reference**
DMT CCN Counter	CCN(s), for either SS=0.43% or SS $\in$ [0.2,0.7%]	ΔSS=0.04, δCCN=10%	Lance, Nenes, Medina, and Smith (2006)
TSI CPC-3772	CN-10nm	10%	/
TSI LAS	dNa/dlogD for D $\in$ [0.1,3.1 um]	20%	Froyd et al. (2019)
SMPS	dNa/dlogD for D $\in$ [0.003,0.089 um]	20%	Moore et al. (2017)
PILS	Mass conc. for D $\in$ [0.05,4.00 um]	/	Sorooshian et al. (2006)
AMS	Mass conc. for D $\in$ [0.06,0.60 um]	<50%	DeCarlo et al. (2008)
SPEC FCDP	dNd/dlogD for D $\in$ [3.0,50 um], LWP	/	Knop, Bansmer, Hahn, and Voigt (2021)
SPEC 2DS	dNd/dlogD for D $\in$ [30,1460 um], LWP, IWC	/	Lawson et al. (2006) Kleine et al. (2018) Taylor et al. (2019)
PICARRO G2401-m	CO gas concentration	2%	/
Instrument (remote)			
HSRL-2	Cloud-top height		Burton et al. (2018)
RSP	Cloud optical thickness, Droplet effective radius	15%	Cairns, Russell, and Travis (1999)
Dropsonde	Temperature, Pressure	0.2 K and 0.05 hPa	Hock and Franklin (1999)

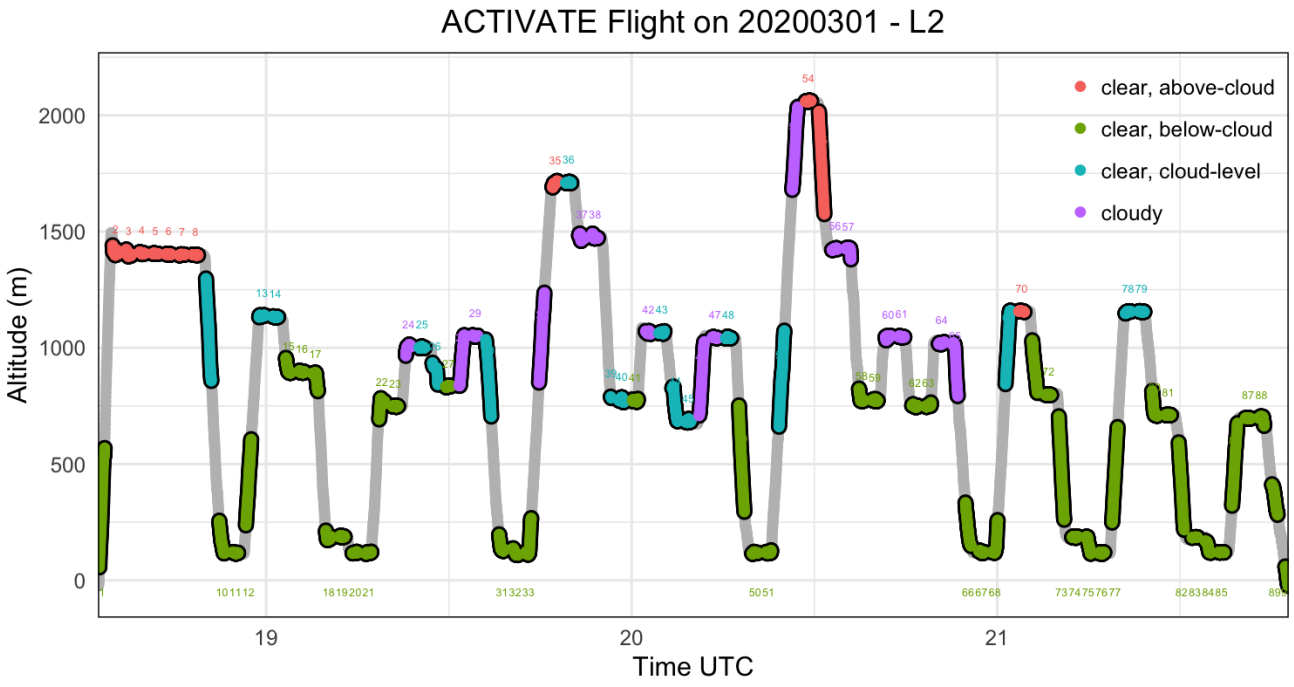

Figure S1. Categorization of CCN measurements during RF14 on 1 March 2020 as defined in Section 2.1.

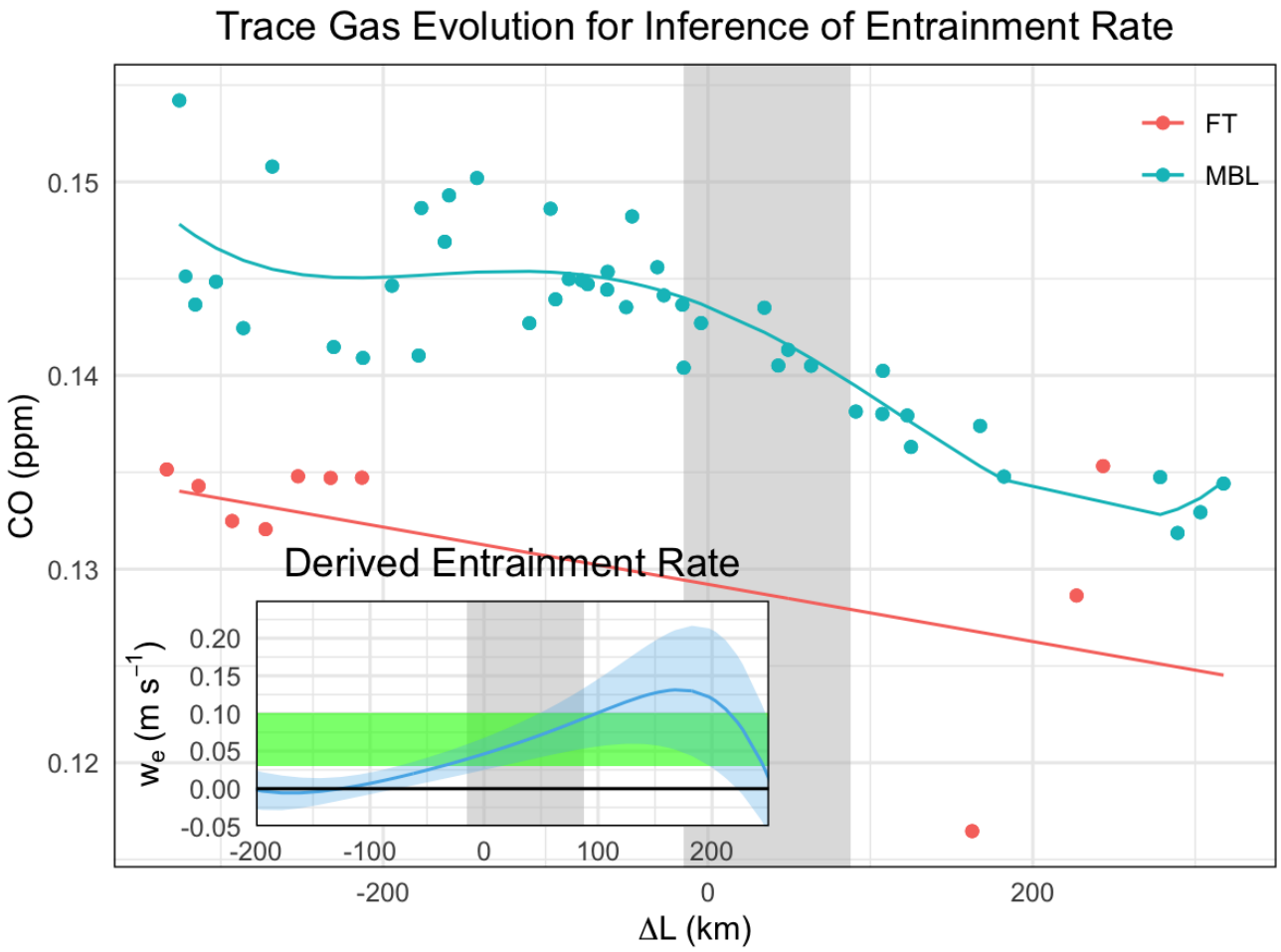

Figure S2. CO trace gas measurements during RF14 on 1 March 2020 as a function of distance from cloud edge (ΔL) sorted into altitudes relative to the cloud deck (see legend). Inset: entrainment rates derived from mixed-layer framework (blue) with shaded uncertainties (plus/minus one sigma), and the range found in large-eddy simulations of a similar case (green shading; Tornow et al., 2021). Gray shading indicates distance range of budget analysis.

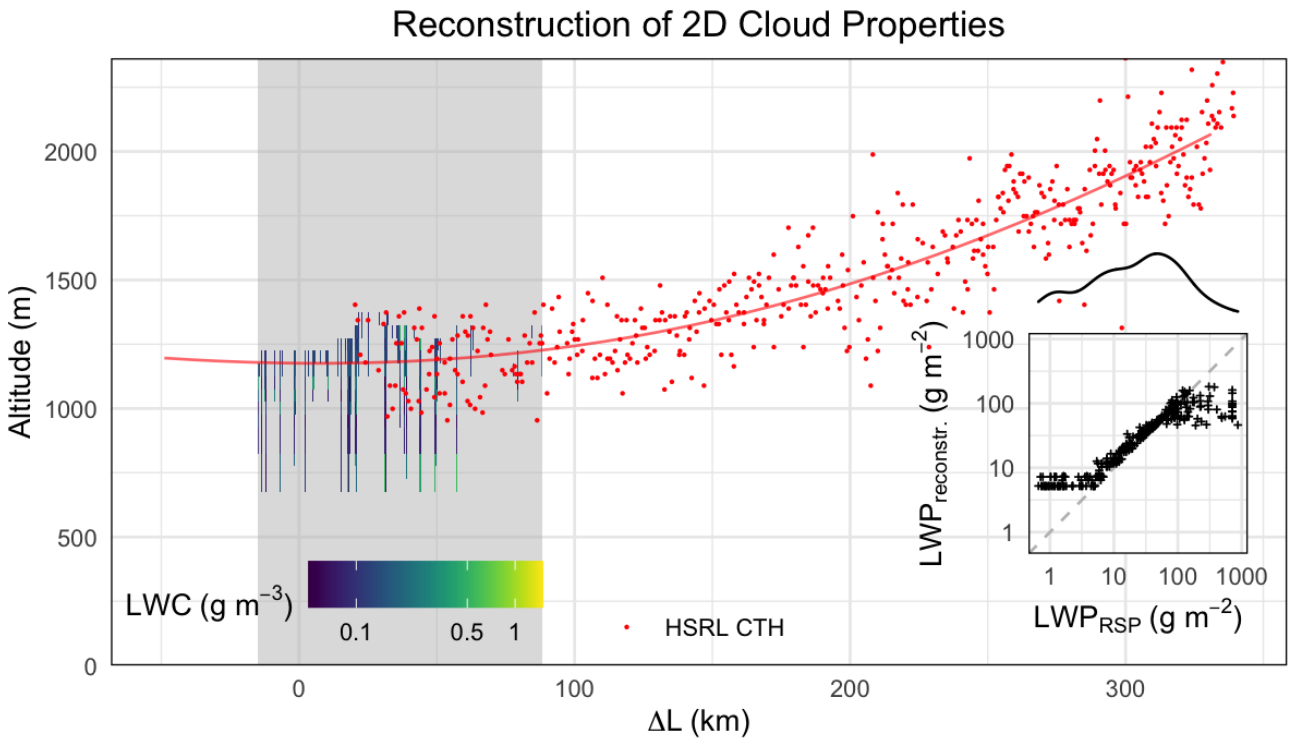

Figure S3. Overview of RF14 (1 March 2020) mock-cloud-profiles (LWC shown as colored shading) together with HSRL-2 cloud-top heights (red). The inset compares LWP from reconstructed profiles with the RSP-based LWP values. The curve above the inset indicates the probability density function for RSP-based values.

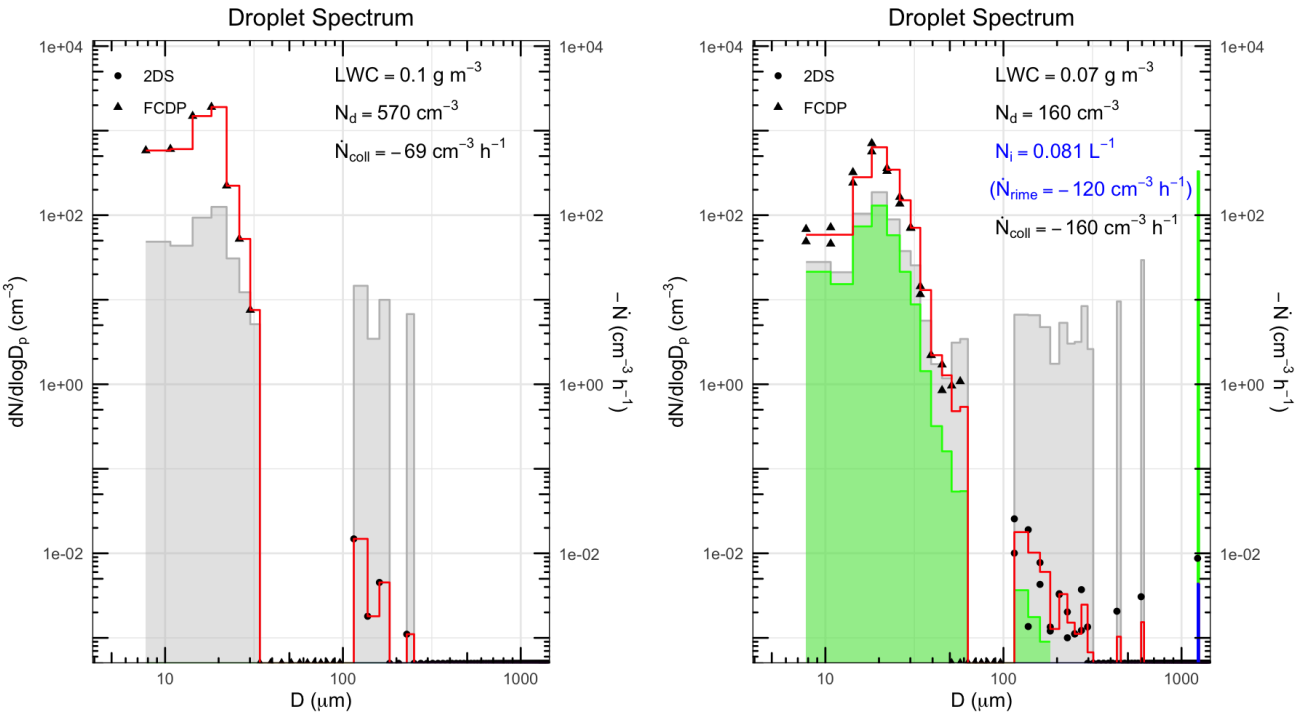

Figure S4. Example hydrometeor size distributions (red, scale on left axes) during RF14 at flight time 70495 s (left) and at 73525 s (right) and corresponding computed collision loss rates (listed at top-right corner) with bin-wise contributions (gray shade, scale on right axes). Rates that involved hydrometeors classified as frozen (only in one bin, shown with blue bar) are labelled as "riming" (shown as integral in blue text and as bin-wise contribution through green shading).

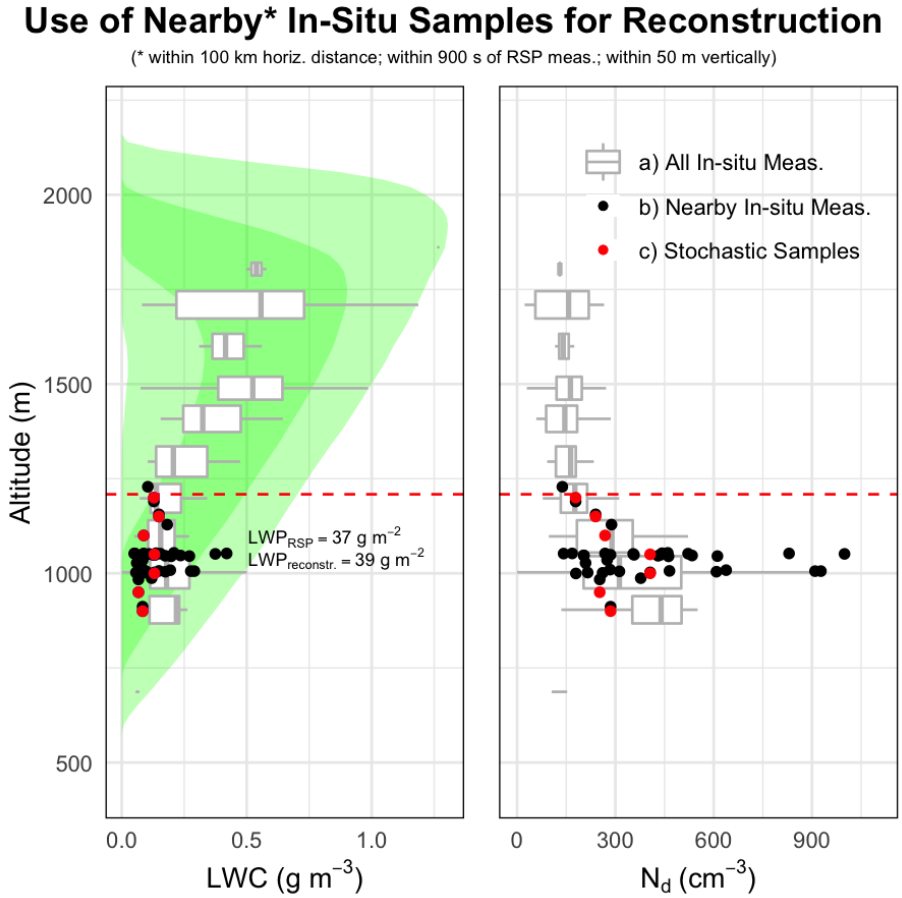

Figure S5. Example of RF14 (1 March 2020) in-situ samples (black) to stochastically build a mock-cloud-profile (red), shown for LWC (left) and N_d (right), until the LWP roughly matches the nearby RSP-sampled value. Gray bars mark the range of all in-situ observations (box ranging between 25$^{\text{th}}$ and 75$^{\text{th}}$ percentiles and whiskers extending to 5$^{\text{th}}$ and 95$^{\text{th}}$ percentiles). The green shading (lighter shade marks 5$^{\text{th}}$ to 95$^{\text{th}}$ and darker shade 25$^{\text{th}}$ to 75$^{\text{th}}$ percentiles) shows LWC profiles from large-eddy simulations of a similar case (altitudes shifted 500 m downward). The decrease of N_d with height is an artifact of MBL deepening downwind where N_d progressively decreases.

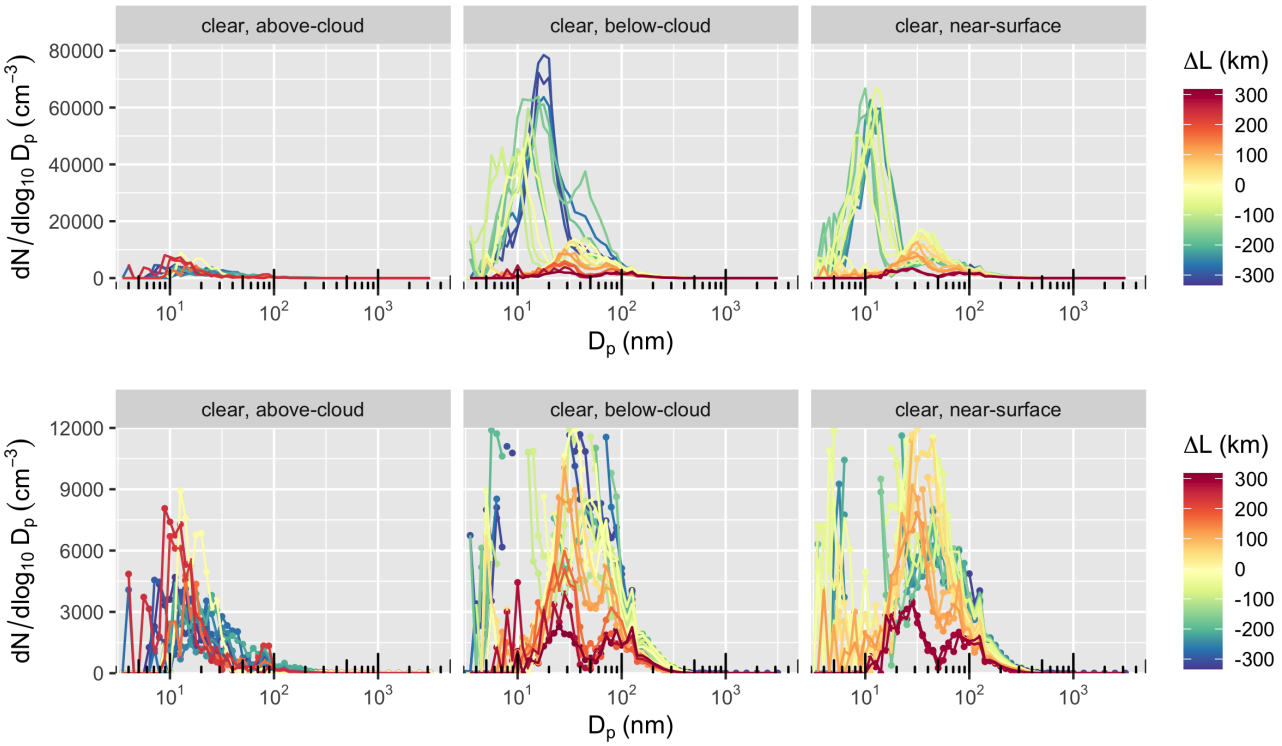

Figure S6. Aerosol particle size distributions measured during RF14 (1 March 2020) in the FT and MBL (top; and with reduced y-axis range, bottom). Colors mark the downwind distance from cloud edge, ΔL.

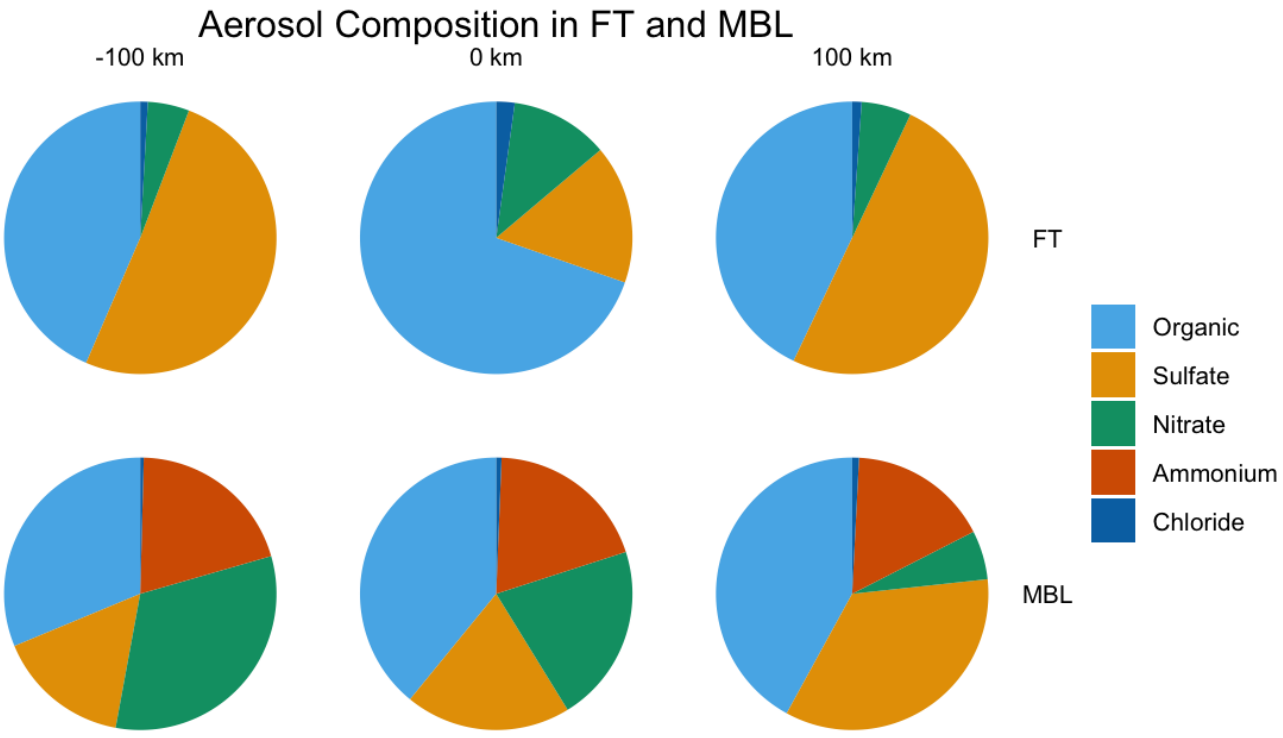

Figure S7. Aerodyne High-Resolution Mass Spectrometer (AMS) measurements during RF14 (1 March 2020) for the approximate size range 60-600 nm, showing mass proportions in FT (top) and MBL (bottom) air masses and were interpolated to three selected ΔL values (horizontal position).

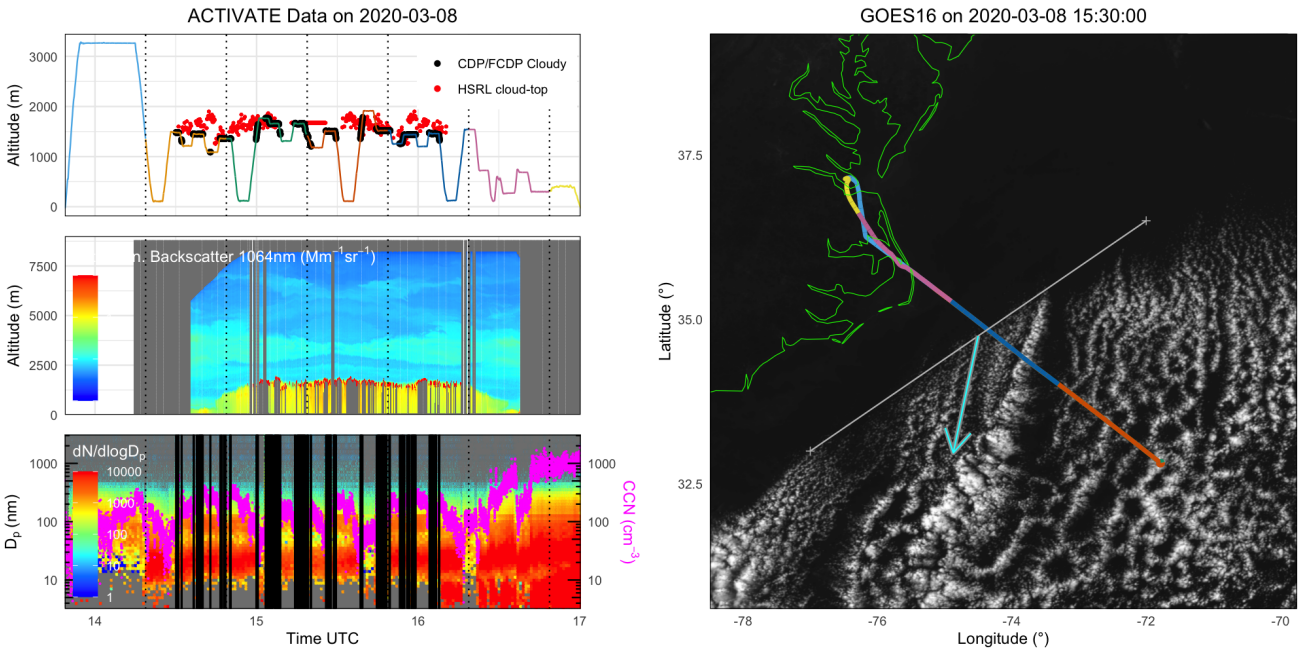

Figure S8. As in Figure 1, but for the first research flight on 8 March 2020 (RF17).

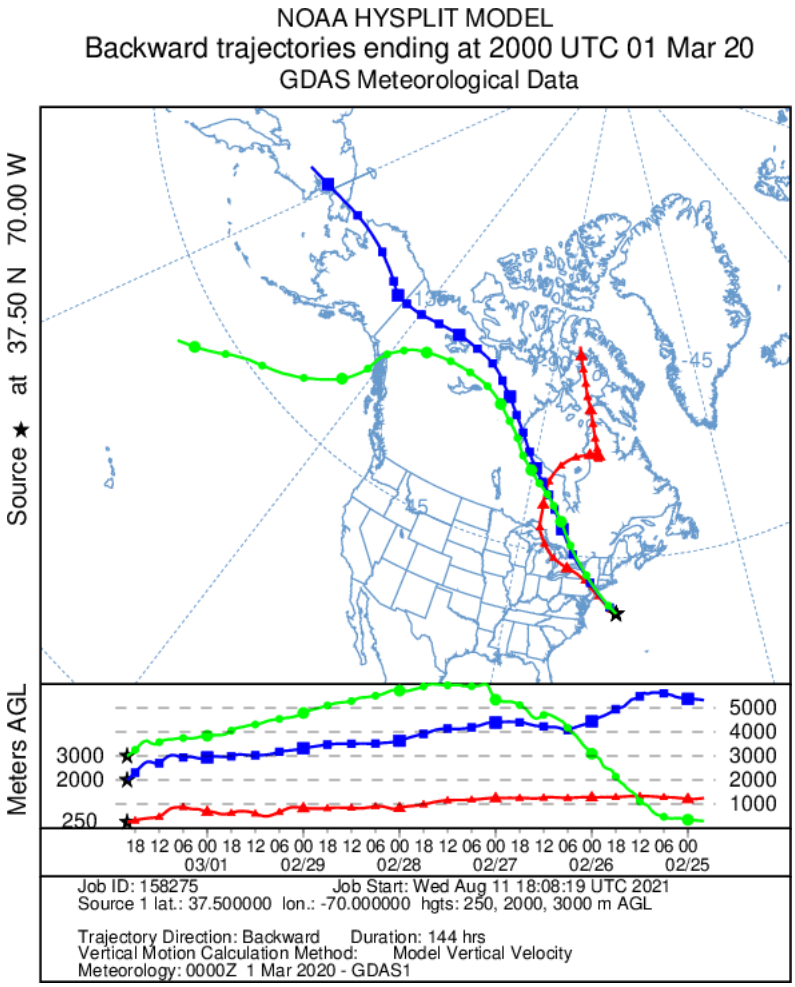

Figure S9. Back-trajectories based on HYSPLIT (Stein et al., 2015; Rolph et al., 2017) for RF14.